Transp Porous Med (2011) 88:169–185
DOI 10.1007/s11242-011-9732-y

Natural Convection Induced by a Centrifugal Force Field in a Horizontal Annular Porous Layer Saturated with a Binary Fluid

Z. Alloui · P. Vasseur

Received: 12 August 2010 / Accepted: 17 January 2011 / Published online: 4 February 2011

Abstract The Darcy Model with the Boussinesq approximation is used to study natural convection in a horizontal annular porous layer filled with a binary fluid, under the influence of a centrifugal force field. Neumann boundary conditions for temperature and concentration are applied on the inner and outer boundary of the enclosure. The governing parameters for the problem are the Rayleigh number, Ra, the Lewis number, Le, the buoyancy ratio, φ, the radius ratio of the cavity, R, the normalized porosity, ε, and parameter a defining double-diffusive convection ($a = 0$) or Soret induced convection ($a = 1$). For convection in a thin annular layer ($R \to 1$), analytical solutions for the stream function, temperature and concentration fields are obtained using a concentric flow approximation and an integral form of the energy equation. The critical Rayleigh number for the onset of supercritical convection is predicted explicitly by the present model. Also, results are obtained from the analytical model for finite amplitude convection for which the flow and heat and mass transfer are presented in terms of the governing parameters of the problem. Numerical solutions of the full governing equations are obtained for a wide range of the governing parameters. A good agreement is observed between the analytical model and the numerical simulations.

Keywords Natural convection · Porous media · Onset of convection · Double diffusion · Soret effect · Finite amplitude convection

List of symbols

D Mass diffusivity of species, m^2/K
D' Thermodiffusion coefficient, m^2/sK
j' Constant mass flux per unit area, kg/ms

Z. Alloui (✉) · P. Vasseur
Ecole Polytechnique, C.P. 6079, Succ "Centre Ville", Montreal, QC H3C 3A7, Canada
e-mail: zineddine.alloui@polymtl.ca
http://www.meca.polymtl.ca/convection

P. Vasseur
Laboratoire des Technologies Innovantes, Université Jules Vernes, 800025 Amiens Cedex, France

K'	Permeability of the porous medium, m^2
k	Thermal conductivity, W/(mK)
Le	Lewis number, (α/D)
N	Mass fraction
N_0	Initial mass fraction of the denser component of the mixture
ΔN	Characteristic mass fraction difference of the reference component
Nu	Nusselt number, Eq. 25
q'	Constant heat flux per unit area, W/m^2
r'	Radius, m
R	Radius ratio, r'_o/r'_i
Ra	Rayleigh number based on the inner radius, $\beta'_T q'_i K' \Omega'^2 r'^4_i / k\alpha\nu$
Ra^*	Rayleigh number based on the gap between inner and outer radius, $Ra(R-1)^2$
Ra_C^{sub}	Subcritical Rayleigh number, Eq. 22
Ra_C^{sup}	Supercritical Rayleigh number, Eq. 24
S	Normalized mass fraction, $N/\Delta N$
Sh	Sherwood number, Eq. 26
t	Dimensionless time, $t'\alpha/(\sigma r'^2_i)$
T	Dimensionless temperature, $(T' - T'_0)/\Delta T'$
T'_0	Reference temperature
ΔT	Characteristic temperature difference, $q'_i r'_i / k$
u	Dimensionless velocity in r direction
v	Dimensionless velocity in θ direction

Greeks

α	Thermal diffusivity, m^2/s
β_N	Concentration expansion coefficient
β'_T	Thermal expansion coefficient
ε	Normalized porosity of the porous medium, ϕ/σ
ν	Kinematic viscosity of fluid, m^2/s
φ	Buoyancy ratio, $(\beta_N \Delta N/\beta'_T \Delta T')$
ρ	Density of fluid, kg/m^3
$(\rho C)_f$	Heat capacity of the fluid, W/K
$(\rho C)_p$	Heat capacity of the saturated porous medium, W/K
σ	Heat capacity ratio, $(\rho C)_p/(\rho C)_f$
θ	Angular coordinate
ϕ	Porosity of the porous medium
Ψ	Dimensionless stream function, Ψ'/α

Subscripts

0	Reference state at position $r = 1, \varphi = \pi/2$
i	Inner cylinder
o	Outer cylinder

Superscript

$'$	Refers to dimensional variable

1 Introduction

The phenomenon of natural convection of a binary fluid through porous media has been recently studied extensively because of its relevance in many natural and technological applications. In industry examples include the migration of moisture in fibrous insulations, the underground disposal of nuclear waste, the contaminant transport in saturated soils, welding processes; thermal insulations, etc (Khanafer and Vafai 2002).

Concerning the convection of binary fluids confined in cavities, as discussed for instance by Bahloul et al. (2003), two types of problems have been considered in the literature. In the first type, called double diffusive convection, the solute gradients in the binary mixture are induced by the solutal boundary conditions applied on the walls of the enclosure. In the second type, the species gradients in the binary solution are induced by the thermal gradients via the Soret effect (cross-diffusion). Thus, for this last situation, the concentration gradients are not the consequence of solutal boundary conditions applied on the system. Rather, it is the heat gradients imposed across an initially homogeneous mixture that induces the concentration gradients. Earlier works on natural convection of binary liquids in porous media are concerned with the stability of a horizontal layer heated and salted from the bottom. To this end Nield (1967), Poulikakos (1986), Taslim and Narusawa (1986), and Malashetty (1993) used linear stability analysis to predict the onset of motion. Criteria for onset of motion, via stationary and oscillatory modes, were derived by these authors for various thermal and solutal boundary conditions. Finite-amplitude convection in a horizontal porous layer saturated by binary liquids has been investigated by Rudraiah et al. (1982), Trevisan and Bejan (1987), Chen and Chen (1993), Mamou and Vasseur (1999), and Bahloul et al. (2003). The stability boundaries which separate regions of different type of motion and the existence of subcritical convection are discussed by these authors. Natural convection of binary fluids confined in a vertical cavity subject to horizontal temperature gradients, has been investigated by Trevisan and Bejan (1985), Trevisan and Bejan (1986), Alavyoon (1993), Alavyoon et al. (1994),Goyeau et al. (1996), Mamou et al. (1995a,b, 1998a,b,c), Marcoux et al. (1999) , Joly et al. (2000), Amahmid et al. (2000), Masuda et al. (2002), Boutana et al. (2004), and Alloui et al. (2010). It was found that, depending on the governing parameter s of the problem, various modes of convection prevails. In the case of opposing flows ($\varphi < 0$), the existence of multiple solutions and oscillating flows was reported.

Although most of the available works related to convection of binary liquids in enclosures are concerned with rectangular cavities a few studies concerning the vertical annular configuration are also available. Double diffusive convection in a two-components mixture confined in a vertical annulus, with constant temperature and concentration differences imposed across the vertical walls, has been studied by Shipp et al. (1993) and Yan and Lin (2001). The influences of the governing parameters on the Nusselt and Sherwood numbers are discussed by the authors for fixed values of curvature ratio and aspect ratio of the enclosure. Similar results have been reported by Chang et al. (1986) in the case of a finite vertical tube. The behaviour of a binary mixture saturating a vertical annular porous subjected to thermogravitational diffusion has been studied by Marcoux and Charrier-Mojtabi (1999). It was assumed that the vertical walls of the cavity are maintained at different and uniform temperatures. An analytical solution, valid in the absence of the solutal contribution, was proposed by these authors to predict the optimal separation conditions. The influence of curvature in the separation process was investigated numerically. Bahloul et al. (2006) investigated analytically and numerically the behaviour of a binary mixture saturating a vertical annular porous medium. Useful approximate expressions have been derived to describe the boundary layer regime. Simplified equations for Nusselt and Sherwood numbers have been obtained for heat-driven

and solute-driven flow regimes. Recently double-diffusive convection in vertical annuluses with opposing temperature and concentration gradients has been investigated numerically, on the basis of a Boltzmann model, by Chen et al. (2010). The influences of ratio of buoyancy forces, aspect ratio and radius ratio on heat and mass transfer are discussed in details.

The purpose of the present investigation is to examine both analytically and numerically natural convection due to a centrifugal force field of a binary mixture confined between two horizontal coaxial cylinders. Both the case of double-diffusion and Soret induced convection are considered. In the present study, both cases of opposing ($\varphi < 0$) and aiding ($\varphi > 0$) buoyancy forces are considered. Although this geometry is common in practice, it has not been nearly as well investigated as the vertical counter part. Available studies on this geometry are only concerned with the case of a single component fluid (Aboubi et al. 1995, 1998). An outline of the paper is as follows. The mathematical formulation is given in Sect. 2. Section 3 describes the numerical method used to solve the problem. The analytical approach for steady state solution is presented and discussed in Sect. 4. The concluding remarks are reported in Sect. 5.

2 Mathematical Formulation

Consider a saturated porous medium filled with a binary mixture contained between concentric cylinders of radius r_i' and r_o', respectively. The annular porous medium, rotating with a constant angular velocity Ω', is subjected to a centrifugal force field which is assumed to be large enough so that the gravity acceleration force can be neglected. The problem is solved in a noninertial coordinate system (r', θ') rotating along with the enclosure, as shown in Fig. 1. The porous medium is considered to be homogeneous and isotropic and in local thermal and compositional equilibrium with the fluid. Uniform heat fluxes, q_o' and q_i', and mass fluxes $(1 - a)j_o'$ and $(1 - a)j_i'$, boundary conditions are applied, for both temperature and concentration, on the inner and outer boundaries, respectively. The case $a = 0$ corresponds to double-diffusive convection for which the solutal buoyancy forces in the annular cavity are induced by the imposition of uniform fluxes of heat and mass on the inner and outer boundaries. On the other hand $a = 1$ corresponds to the case of a binary fluid subject to the Soret effect. All the boundaries are hydrodynamically impermeable.

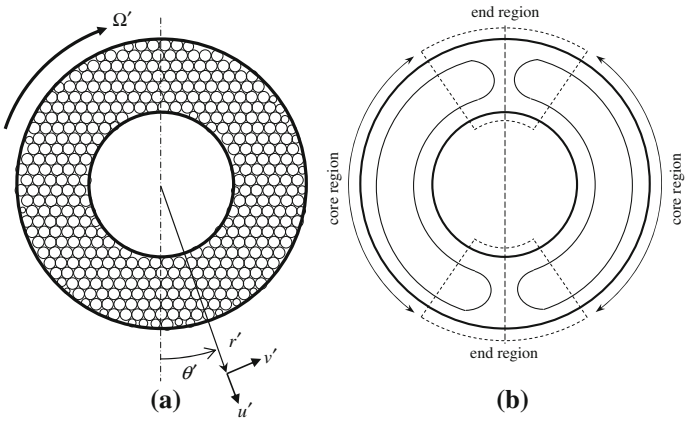

Fig. 1 Schematic diagram of the problem domain and coordinate system

The binary fluid is assumed to be Newtonian and to satisfy the Boussinesq approximation. The density variation with temperature and concentration is described by the state equation $\rho = \rho_0[1 - \beta'_{\mathrm{T}}(T' - T'_0) - \beta_N(N - N_0)]$ where ρ_0 is the fluid mixture density at temperature $T' = T'_0$ taken arbitrarily at position ($r = 1, \theta = \pi/2$) and mass fraction of the reference component $N = N_0$. β'_{T} and β_N are the thermal and mass species expansion coefficients, respectively. The mass fraction of the denser component of the mixture, N_0, is assumed to be initially uniform.

The phenomenological equations relating the flux of heat $\vec{Q}'$ and matter $\vec{j}'$ to the thermal and solute gradients present in a binary fluid mixture are given by (see for instance, De Groot and Mazur 1969):

$$\vec{Q}' = -k\nabla T' \tag{1}$$

$$\vec{J}' = -\rho D\nabla N - a\rho D' N_0 (1 - N_0) \nabla T' \tag{2}$$

where k and D are the thermal conductivity and the molecular (or isothermal) diffusion coefficient of species and D' the thermodiffusion coefficient. The second term, in the right hand side of Eq. 2, describes the Soret effect, i.e., mass separation due to a temperature gradient.

In the present study, the Dufour effect, i.e., heat transfer driven by a concentration gradient, is neglected as usual. This parameter can be important in binary gas mixtures but is negligible in binary liquid mixture.

The governing equations which describe the system behaviour are conservation of momentum, energy and species which are given below in terms of the stream function Ψ as:

$$\nabla^2\Psi = -Ra\left(\frac{\partial T}{\partial\theta} + \varphi\frac{\partial S}{\partial\theta}\right) \tag{3}$$

$$\nabla^2 T = \frac{\partial T}{\partial t} + \frac{1}{r}J(\Psi, T) \tag{4}$$

$$\frac{1}{Le}\left(\nabla^2 S - a\nabla^2 T\right) = \varepsilon\frac{\partial S}{\partial t} + \frac{1}{r}J(\Psi, S) \tag{5}$$

where, as usual, in order to satisfy the continuity equation, the stream function Ψ is defined such that $u = (1/r)(\partial\Psi/\partial\theta)$, $v = -\partial\Psi/\partial r$ and $\nabla^2 f = (1/r)\partial(r\partial f/\partial r)/\partial r + (1/r^2)(\partial^2 f/\partial\theta^2)$, $J(f, g) = \partial f/\partial\theta\partial g/\partial r - \partial f/\partial r\partial g/\partial\theta$.

The above equations have been reduced to dimensionless form by introducing the following scales

$$r = r'/r'_{\mathrm{i}}, \quad \Psi = \Psi'/\alpha, \quad t = t'\alpha/\left(\sigma r'^2_{\mathrm{i}}\right), \quad T = (T' - T'_0)/\Delta T', \quad S = N/\Delta N \tag{6}$$

where $\Delta T' = q'_{\mathrm{i}} r'_{\mathrm{i}}/k$ and $\Delta N = -j'_{\mathrm{i}}/\rho D$ for double diffusive convection and $\Delta N = N_0(1 - N_0)\Delta T' D'/D$ for Soret-driven convection. Other symbols are defined in the nomenclature.

Assuming flow symmetry about the vertical centerline, the dimensionless boundary conditions applied on the walls of the system are

$$\Psi = 0; \quad \frac{\partial T}{\partial r} = 1, 1/R; \quad \frac{\partial S}{\partial r} = (a - 1) + a\frac{\partial T}{\partial r} \quad \text{for } r = 1, R \tag{7}$$

$$\Psi = 0; \quad \frac{\partial T}{\partial\theta} = 0; \quad \frac{\partial S}{\partial\theta} = 0 \quad \text{for } \theta = 0, \pi \tag{8}$$

From the above equations it is observed that the present problem is governed by the Rayleigh number $Ra = \beta'_{\mathrm{T}} q'_{\mathrm{i}} K' \Omega'^2 r'^4_{\mathrm{i}}/k\alpha\nu$ based on inner heat flux and centrifugal force field,

buoyancy ratio $\varphi = \beta_N \Delta N / \beta'_T \Delta T'$, Lewis number $Le = \alpha / D$, radius ratio $R = r'_o / r'_i$, the normalized porosity $\varepsilon = \phi / \sigma$ and parameter a.

The heat and mass transfer rates can be expressed in terms of the Nusselt and Sherwood numbers, and can be obtained from the following expressions:

$$Nu = \frac{\Delta T_C}{\Delta T} \tag{9}$$

$$Sh = \frac{\Delta S_C}{\Delta S} \tag{10}$$

where $\Delta T = T(R) - T(1)$ and $\Delta S = S(R) - S(1)$ are the dimensionless temperature and concentration differences, while ΔT_C and ΔS_C stands for the rest state regime. Since ΔT_C and ΔS_C are independent of θ it was evaluated arbitrary at the position $\theta = \pi/2$ in the numerical procedure.

3 Numerical Solution

The solution of the governing equations (3–5) and boundary conditions (7–8) is obtained using a control volume approach and SIMPLER algorithm (Patankar 1980). A finite difference procedure with constant grid size is considered. The power-law scheme is used to evaluate the flow, heat, and mass fluxes across each of the control volume boundaries. A second order back-wards finite difference scheme is employed to discretize the temporal terms appearing in the governing equations.

A line-by-line tridiagonal matrix algorithm with relaxation is used in conjunction with iterations to solve the nonlinear discretized equations. We consider that convergence is reached when

$$\frac{\sum_i \sum_j \left| \Psi_{i,j}^{n+1} - \Psi_{i,j}^{n} \right|}{\sum_i \sum_j \left| \Psi_{i,j}^{n+1} \right|} \leq 10^{-6} \tag{11}$$

where the superscripts n and $(n+1)$ indicate the value of the nth and $(n+1)$th iterations respectively, i and j indices denote grid location in the (x, y) plane. Numerical tests, using various mesh sizes, were done for the same conditions in order to determine the best compromise between accuracy of the results and computer time. Thus, in general, the calculations presented in this paper were performed using a 60×180 grid. The criteria of convergence are to conserve momentum, energy, and species globally and to insure convergence of preselected dependent variables to constant values within machine error at each time step.

Typical numerical results are presented in Fig. 2a–c for $Ra^* = 50$, $\varphi = 0.02$, $Le = 10$, $a = 0$, and $R = 1.2, 3$, and 10 respectively. The modified Rayleigh number, $Ra^* = Ra(R-1)^2$, is used here for convenience. On the graphs streamlines, isotherms and isoconcentrates are presented from left to right, respectively. The flow inside the cavity is separated in two distinct counterotating cells that are symmetrical with respect to the vertical axis of the cavity. The results illustrate clearly the dependence of the present problem on the radius ratio R. Thus, when R is small enough ($R = 1.2$), Fig. 2a shows that the flow in the core region of the cavity is essentially parallel while the temperature and concentration in the core are linearly stratified in the azimuth direction. Naturally, near the top and the bottom of the enclosure the flow turns through 180° and is more complex. The analytical solution, developed in the following section, will rely on these observations. As the radius ratio R is made larger it is

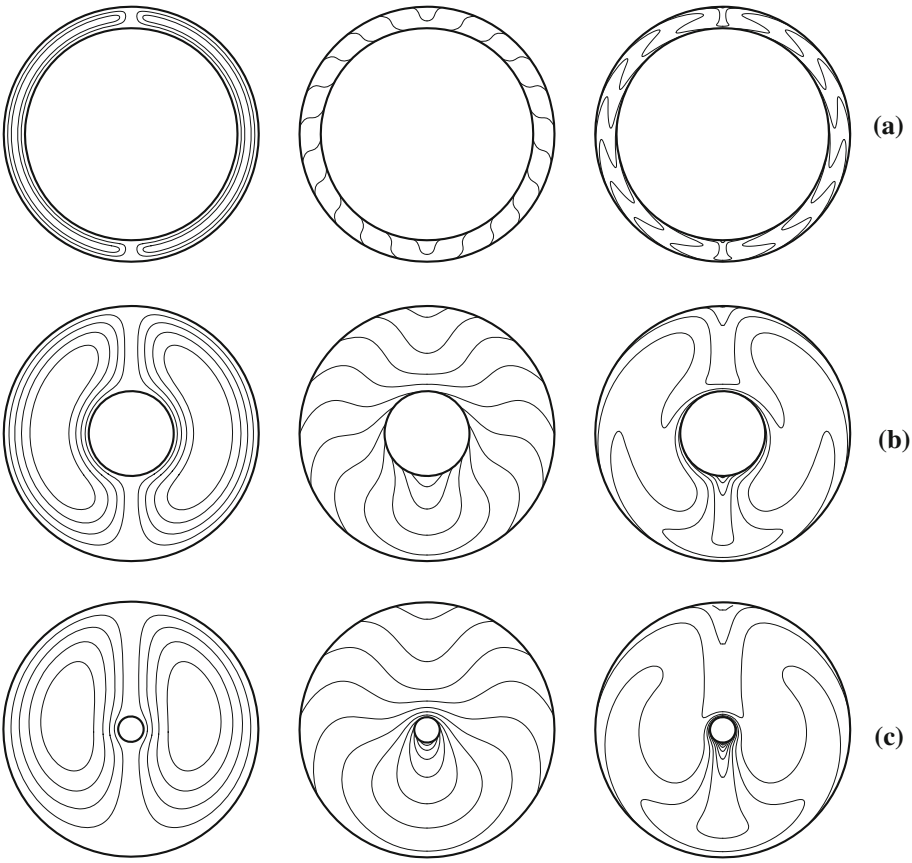

Fig. 2 Contour lines of stream function (*left*), temperature (centre) and concentration (*right*) for $Ra^* = 50$, $a = 0$, $Le = 10$ and $\varphi = 0.02$. **a** $R = 1.2$, $\Psi_{\max} = 2.44$, $Nu = 2.73$, $Sh = 5.88$. **b** $R = 3$, $\Psi_{\max} = 2.52$, $Nu = 2.72$, $Sh = 6.84$. **c** $R = 10$, $\Psi_{\max} = 2.51$, $Nu = 2.20$, $Sh = 7.49$

clear from Fig. 2b and c that the parallelism of the flow is progressively destroyed. This is illustrated by the streamlines of Fig. 2c for the case $R = 10$.

In the present study, numerical tests have been performed to determine the maximum radius ratio below which the flow can be assumed parallel. Typical results are presented in

Table 1 Comparison of the analytical and the numerical results for the case $\varphi = 0$

	$R = 2$		$R = 3$		$R = 4$		$R = 5$	
	Nu	$\Psi_{\max}$	Nu	$\Psi_{\max}$	Nu	$\Psi_{\max}$	Nu	$\Psi_{\max}$
$Ra^* = 50$								
Analytical	2.725	2.458	2.722	2.489	2.720	2.518	2.718	2.544
Numerical	2.725	2.459	2.717	2.519	2.658	2.562	2.575	2.574
$Ra^* = 75$								
Analytical	3.322	3.164	3.307	3.202	3.293	3.237	3.282	3.268
Numerical	3.320	3.165	3.297	3.235	3.233	3.293	3.141	3.318

Table 1 for the case $\varphi = 0$, $Ra^* = 50$ and 75. It is found that for $R \leq 4\Psi_{\max}$ and Nu tend toward the values predicted by the analytical solution which will be derived in the following section. Naturally, this result depends slightly upon the governing parameters of the problem. For this reason, in order to be on the safe side, all the numerical results presented in this paper are restricted to the case $R \leq 3$.

4 Analytical Solution

In the limit of a thin annular cavity, the governing Eqs. 3–5 can be considerably simplified under the concentric flow assumption. As illustrated in Fig. 2a for $R \to 1$ the flow pattern in the cavity consists of two counter rotating cells symmetrical with respect to a vertical plane ($\theta = 0$). As illustrated schematically in Fig. 1b the flow pattern in each cell consists in a core region, where the flow is concentric ($u = 0, v = v(r)$), and two end regions, near $\theta \simeq 0, \pi/2$, where the flow turns trough 180°. In the core region, the flow is essentially one-dimensional and it is assumed that $\Psi(r,\theta) \approx \Psi(r)$, $T(r,\theta) \approx C_T\theta + \Theta_T(r)$ and $S(r,\theta) \approx C_S\theta + \Theta_S(r)$, where C_T and C_S are unknown constant temperature and concentration gradients, respectively, in θ-direction. These approximations are similar than those used in the case of a shallow cavity (see for instance Mamou et al. 1995a,b).

Using the above approximations, Eqs. 3–5 reduce to the following systems of equations

$$\frac{1}{r}\frac{\mathrm{d}}{\mathrm{d}r}\left(r\frac{\mathrm{d}\Psi}{\mathrm{d}r}\right) = -Ra(C_T + \varphi C_S) \tag{12}$$

$$\frac{\mathrm{d}}{\mathrm{d}r}\left(r\frac{\mathrm{d}\Theta_T}{\mathrm{d}r}\right) = -C_T\frac{\mathrm{d}\Psi}{\mathrm{d}r} \tag{13}$$

$$\frac{\mathrm{d}}{\mathrm{d}r}\left(r\frac{\mathrm{d}\Theta_S}{\mathrm{d}r}\right) - a\frac{\mathrm{d}}{\mathrm{d}r}\left(r\frac{\mathrm{d}\Theta_T}{\mathrm{d}r}\right) = -LeC_S\frac{\mathrm{d}\Psi}{\mathrm{d}r} \tag{14}$$

The solution of Eqs. 12–14, satisfying the boundary conditions (7) is:

$$\Psi(r) = \Psi_0 F(r) \tag{15}$$

$$\Theta_T(r) = \ln(r) + C_T\Psi_0 G(r) \tag{16}$$

$$\Theta_S(r) = \ln(r) + (aC_T + LeC_S)\Psi_0 G(r) \tag{17}$$

where $\Psi_0 = Ra(C_T + \varphi C_S)$, and functions $F(r)$ and $G(r)$ are defined by

$$F(r) = \left[\left(1 - r^2\right) - \left(1 - R^2\right)\ln(r)/\ln(R)\right]/4 \tag{18}$$

$$G(r) = \left[\left(1 - r^2\right) + \ln(r)\left[2 - \left(1 - R^2\right)\ln(r)/\ln(R)\right]\right]/8 \tag{19}$$

The effect of the return flow from the end regions is taken into account via a global balance (see, for instance, Trevisan and Bejan 1986). Making use of the boundary conditions, Eq. 7, the temperature and concentration gradients C_T and C_S can be obtained as:

$$C_T = \frac{A_1\Psi_0}{\left(A_2\Psi_0^2 + A_3\right)} \tag{20}$$

$$C_S = \frac{-aC_T\left(A_2Le\Psi_0^2 - A_3\right) + A_1Le\Psi_0}{\left(A_2Le^2\Psi_0^2 + A_3\right)} \tag{21}$$

where:

$$A_1 = 24\ln(R)\left[\ln(R) + R^2\ln(R) - R^2 + 1\right],$$
$$A_2 = 9(1-R^4)\ln(R) + 4(R^4 + R^2 + 1)\ln(R)^2 + 6(R^4 - 2R^2 + 1),$$
$$A_3 = 192\ln(R)^2$$

Substituting the above equations of C_T and C_S into the expression for Ψ_0, the following fifth order polynomial is obtained:

$$\Psi_0\left[Le^4\Psi_0^4 - 2Le^2 d_1\Psi_0^2 - d_2\right] = 0 \tag{22}$$

where:

$$\left.\begin{array}{l} d_1 = \frac{1}{2A_2^2}\left\{RaLeA_1A_2\left[Le + \varphi(1-a)\right] - A_2A_3(Le^2+1)\right\} \\ d_2 = \frac{1}{A_2^2}\left\{RaA_1A_3\left[1 + \varphi(Le+a)\right] - A_3^2\right\}Le^2 \end{array}\right\} \tag{23}$$

The solution for Eq. 23 is explicitly expressed as follows:

$$\Psi_0 = \left\{\pm\frac{1}{Le}\left(d_1 \pm \sqrt{d_1^2 + d_2}\right)^{1/2}, 0\right\} \tag{24}$$

in which the solution $\Psi_0 = 0$ represents the pure conduction rest state and the four other solutions stand for convective solutions.

The analytic model also predicts the onset of convection from the rest state ($\Psi_0 = 0$) to convection ($\Psi_0 \neq 0$). For the present situation two types of bifurcation are possible. The first transition, called supercritical bifurcation, is characterized by a transition from the rest state to the convection regime occurring through zero flow amplitude. This threshold is obtained, when the conditions $d_1 < 0$ and $d_2 = 0$ are satisfied, at a supercritical Rayleigh number Ra_C^{sup} given by

$$Ra_C^{sup} = \frac{Ra_0}{\left[1 + \varphi(Le+a)\right]} \tag{25}$$

where

$$Ra_0 = A_3/A_1 \tag{26}$$

The second transition, called subcritical bifurcation, is characterized by a transition from the rest state to a finite amplitude convection of magnitude $\Psi_0 = \pm\sqrt{d_1}/Le$. The subcritical Rayleigh number Ra_C^{sub} is obtained from the conditions $d_1 > 0$ and $d_1^2 + d_2 = 0$ as

$$Ra_C^{sub} = \frac{(1+Le)\,Ra_0}{Le\left[Le + \varphi\,(1-a)\right]^2}\left\{\begin{array}{l}(Le-1)\,(Le-\varphi) - a\varphi\,(Le+1) \\ +2\sqrt{\varphi Le\,(Le+a-1)\,(a\varphi - Le + 1)}\end{array}\right\} \tag{27}$$

The local heat and mass transfer rates are obtained according, to Eqs. 9, 10, 16, and 17, by:

$$Nu = \frac{1}{1 - C_T\Psi_0 B} \tag{28}$$

$$Sh = \frac{1}{1 - (LeC_S + aC_T)\Psi_0 B} \tag{29}$$

where

$$B = \left[\ln(R) + R^2\ln(R) - R^2 + 1\right]/\left[8\ln(R)\right] \tag{30}$$

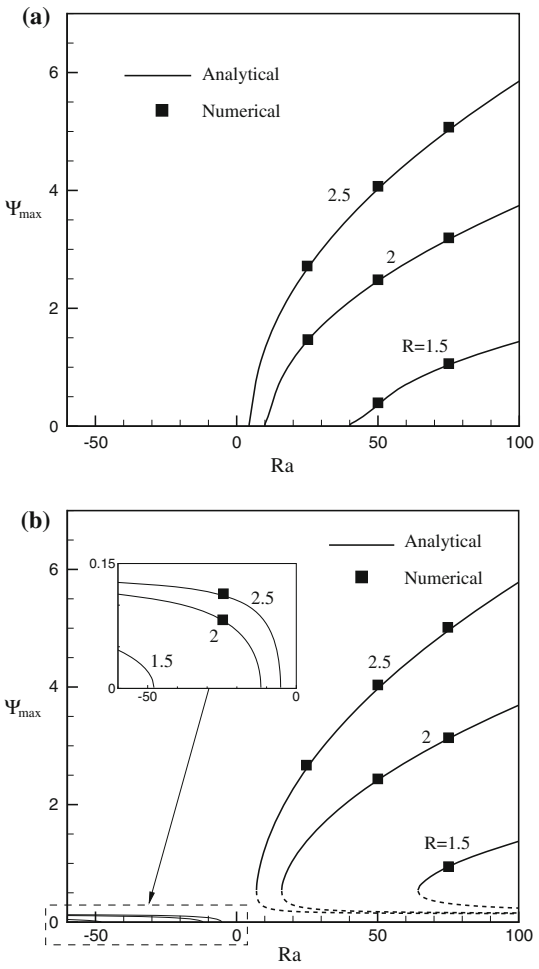

Fig. 3 Bifurcation diagrams in terms of Ψ_{max} versus Ra for $Le = 10$, $a = 0$ and for various values of R: **a** $\varphi = 0.02$ and **b** $\varphi = -0.5$

From the above solution, the special case of a horizontal porous layer heated from below by a constant heat flux ($R \rightarrow 1$), as considered recently by Bahloul et al. (2003), can be recovered.

Some typical analytical and numerical results are presented in Fig. 3, in terms of bifurcation diagrams of the maximum streamfunction (Ψ_{max}) versus the Rayleigh number (Ra), for $Le = 10$, $a = 0$, i.e., double diffusive convection, and various values of R. The curves depicted in the graphs are the prediction of the concentric flow approximation. The numerical solutions of the full governing equations, depicted by symbols, are seen to be in good agreement with the analytical solution. The results corresponding to the case of aiding flows ($\varphi = 0.02$), in which the heat and solute are destabilizing, are depicted in Fig. 3a. For this situation the onset of motion is supercritical and occurs through a pitchfork bifurcation. Naturally, the flow circulation can be indifferently clockwise ($\Psi_{max} < 0$) or counterclockwise ($\Psi_{max} > 0$) and only the counterclockwise solution is depicted in the graph. As the radius ratio of the cavity R is increased it is observed that the onset of convection occurs at a lower supercritical Rayleigh number as predicted by Eq. 25. Thus, $Ra_C^{sup} = 39.89$ for $R = 1.5$

and $Ra_C^{sup} = 4.38$ for $R = 2.5$. Also, the results indicate that for a given Rayleigh number, Ra, the intensity of convective flow is promoted by an increase of the radius ratio R. Typical results, obtained for the case of opposing flows, in which the heat is destabilizing and the solute is stabilizing, are presented in Fig. 3b for the case $\varphi = -0.5$. For this situation the onset of motion occurs at subcritical Rayleigh number, Ra_C^{sub}, well below the supercritical Rayleigh number Ra_C^{sup}. The analytical solutions depicted by solid lines, referred to as stable branches, are confirmed by the numerical solution. This is not the case of the dotted lines, connecting the subcritical and supercritical Rayleigh number, which correspond to an unstable solution. It is noted that in the subcritical regime, the transition from the rest state to the convective mode occurs through finite-amplitude convection. For the conditions considered here the onset of subcritical convection occurs at $Ra_C^{sub} = 78.62$ for $R = 1.5$ and $Ra_C^{sub} = 8.64$ for $R = 2.5$. The results obtained for $Ra < 0$, corresponding to the case when the inner cylinder is now heated while the outer cylinder is cooled, are also presented in Fig. 3b. For this situation, convection occurs through a pitchfork bifurcation at a supercritical Rayleigh number Ra_C^{sup} given by Eq. 25. It is noted that results obtained for $a = 1$ (Soret-induced convection) were found to be qualitatively similar to those reported above. For this reason, they are not presented here.

Figure 4a–c exemplifies the differences between double diffusive convection ($a = 0$) and Soret-induced convection ($a = 1$) for $R = 2$, $Le = 2$, and $Le = 10$. The case of pure thermal convection ($\varphi = 0, a = 0$), presented for comparison purpose, corresponds, to a classical Bénard situation. It gives rise to a supercritical Rayleigh number $Ra_C^{sup} = 11.9$, as predicted by Eq. 25. The way that this pitchfork bifurcation is affected by the solutal buoyancy forces is presented in Fig. 4a for $\varphi = 0.5$ for which the thermal and solutal forces are destabilizing. The results show that pitchfork bifurcations are obtained at $Ra_C^{sup} = 5.95$ for double-diffusive convection ($a = 0$) and $Ra_C^{sup} = 4.76$ for Soret-induced convection ($a = 1$). The results obtained for $\varphi = -0.5$ are presented in Fig. 5a–c. For this situation, for which the thermal and solutal forces are opposing each other, the graph indicates the occurrence of subcritical bifurcations as already discussed. For the conditions considered here $Ra_C^{sub} = 35.72$ for $a = 0$ and $Ra_C^{sub} = 33.33$ for $a = 1$. For $Ra < 0$ the graphs indicate the occurrence of a supercritical bifurcation, at $Ra_C^{sup} = -23.81$, for Soret-induced convection. The corresponding phenomenon, for double diffusive convection, is not presented here since it occurs at a Rayleigh number out of the range of the present graph.

Figure 6a and b exemplifies the bifurcation diagrams in terms of Nu and Sh, respectively, versus the Rayleigh number Ra and the radius ratio R, for the case $Le = 2$, $\varphi = 0.02$ and $a = 0$. Here again, the curves depicted in these graphs are the prediction of the concentric flow approximation. The numerical solution of the full governing equations, depicted by dots, is seen to be in excellent agreement with analytical solution. In general, it is found that, as expected, both Nu and Sh are observed to increase as the Rayleigh number is made larger

Figure 7a illustrates the time history of Ψ_{max} obtained numerically for the case $Ra = 560$, $R = 2$, $Le = 10$, $\varphi = -0.2$, $a = 0$ and various values of the normalized porosity ε. For $\varepsilon = 0.3$ the numerical results indicate that the flow is steady. However, upon increasing slightly the normalized porosity up to $\varepsilon = 0.33$ the graphs indicates the occurrence of an oscillating flow composed of a single fundamental peak. The intensity of this oscillating motion is observed to be considerably promoted as the porosity of the porous medium is increased to $\varepsilon = 0.35$, i.e., only by 6%. The flow pattern obtained for $\varepsilon = 0.8$, Fig. 7b, indicates that this latter consists of a combination of two large concentric cells and small cells, in the core, growing and decreasing in size with time. This oscillating motion is now composed of two fundamental peaks.

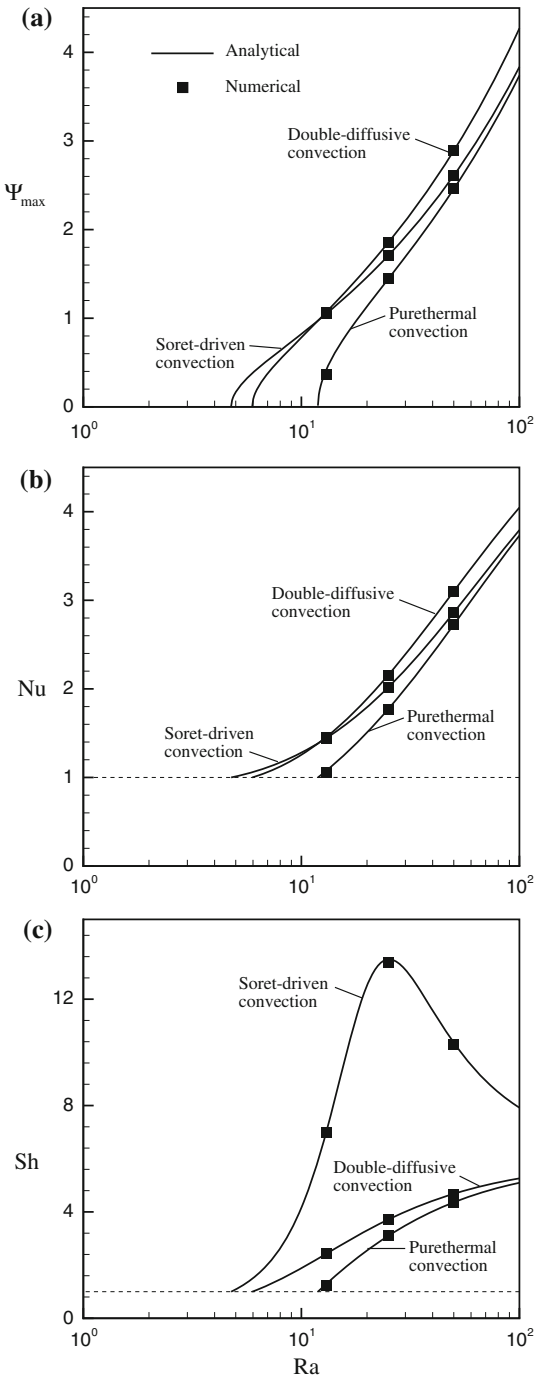

Fig. 4 Bifurcation diagrams in terms of **a** Ψ_{max}, **b** Nu, **c** Sh, versus Ra for $a = 0$ and 1, $R = 2$, $Le = 2$ and $\varphi = 0.5$

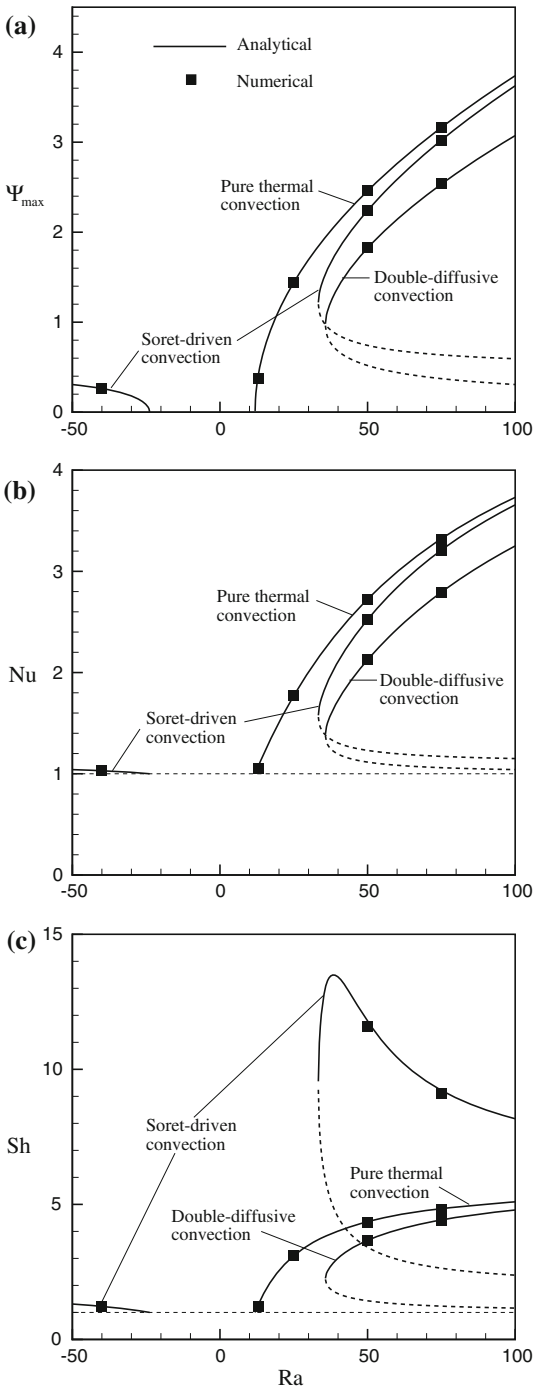

Fig. 5 Bifurcation diagrams in terms of **a** $\Psi_{\max}$, **b** Nu, **c** Sh, versus Ra for $a = 0$ and 1, $R = 2$, $Le = 2$ and $\varphi = -0.5$

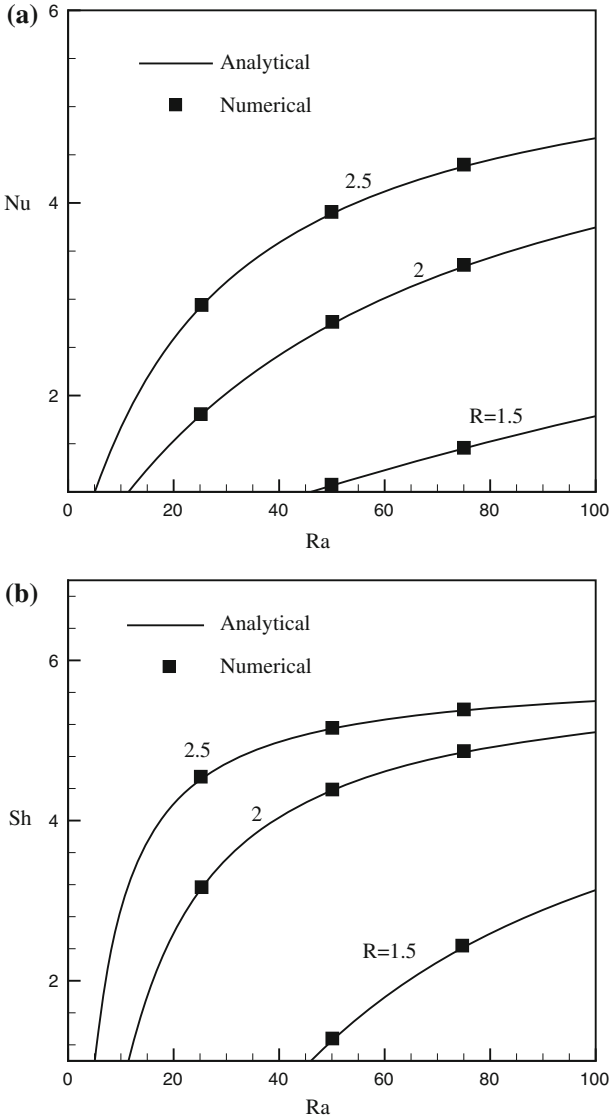

Fig. 6 Bifurcation diagrams in terms of Nu and Sh versus Ra for $Le = 2$, $a = 0$, $\varphi = 0.02$ and for various values of R

5 Conclusions

The onset and development of natural convection in a horizontal annular porous layer, filed with a binary fluid and subjected to a centrifugal force field, is studied both analytically and numerically. The case of double-diffusion convection ($a = 0$) and Soret-driven convection ($a = 1$) are both considered. The governing parameters of the problem are the Rayleigh number, Ra, buoyancy ratio, φ, Lewis number, Le, radius ratio, R, and parameter a. The main conclusions of the present analysis are as follows:

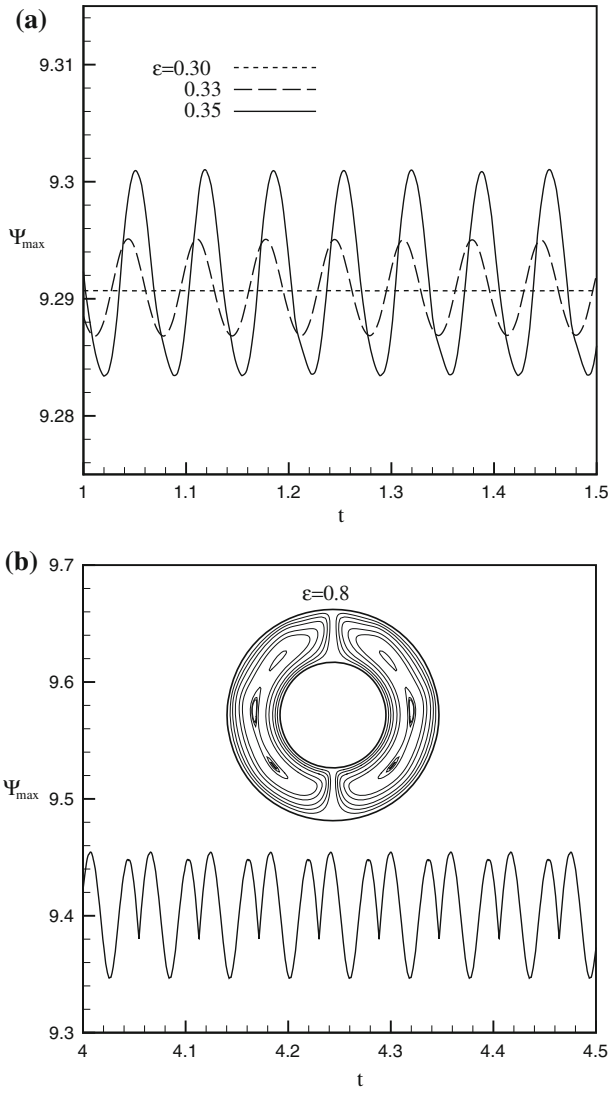

Fig. 7 Time history of the stream function extrema obtained for $Ra = 560, R = 2, a = 0, Le = 10, \varphi = -0.2$ and **a** $\varepsilon = 0.3, 0.33, 0.35$, **b** $\varepsilon = 0.8$

(i) An analytical solution, based on a concentric flow approximation, has been derived in the limit of a thin annular layer ($R \to 1$). For the case of aiding buoyancy forces ($\varphi > 0$) the resulting nonlinear model yields the supercritical Rayleigh number for the onset of convection from the rest state. For opposing flows, ($\varphi < 0$) it predicts the existence of a subcritical branch, where the flow bifurcates from the rest state through finite amplitude convection. Explicit expressions for the supercritical and subcritical Rayleigh numbers are obtained in terms of R, φ, Le, and a. For finite amplitude convection closed form expressions are given for velocity, temperature, and concentration. Also, the effects of the governing parameters on the Nusselt and

Sherwood numbers are predicted. The approximate model, despite its relative simplicity, predicts successfully the flow patterns encountered in the present study. This covers aiding flows and opposing flows.

(ii) A control volume method has been used to obtain a numerical solution of the full governing equations. A good agreement is observed between the analytical predictions and the numerical simulations.

The present study is restricted to flow configuration consisting in two cells. However, it is well known that upon increasing the intensity of convection flow patterns consisting of many pairs of cells are possible.

References

Aboubi, K., Robillard, L., Bilgen, E.: Convective heat transfer in an annular porous layer with centrifugal force field. Num. Heat Transf. **28**, 375–388 (1995)

Aboubi, K., Robillard, L., Vasseur, P.: Natural convection in horizontal annulus filled with an anisotropic porous medium. Int. J. Numer. Methods Heat Fluid Flow **8**, 689–702 (1998)

Alavyoon, F.: On natural convection in vertical porous enclosures due to prescribed fluxes of heat and mass at the vertical boundaries. Int. J. Heat Mass Transf. **36**, 2479–2498 (1993)

Alavyoon, F., Masuda, Y., Kimura, S.: On natural convection in vertical porous enclosures due to opposing fluxes of heat and mass prescribed at the vertical walls. Int. J. Heat Mass Transf. **37**, 195–206 (1994)

Alloui, Z., Merabtine, A., Vasseur, P.: Soret and thermosolutal effects on natural convection in a vertical cavity filled with a binary mixture. Can. J. Chem. Eng. (2010) (under press)

Amahmid, A., Hasnaoui, M., Mamou, M., Vasseur, P.: On the transition between aiding and opposing double-diffusive flows in a vertical porous matrix. Int. J. Porous Med. **3**, 123–137 (2000)

Bahloul, A., Boutana, N., Vasseur, P.: Double-diffusive and Soret-induced convection in a shallow horizontal porous layer. J. Fluid Mech. **491**, 52–325 (2003)

Bahloul, A., Yahiaoui, M.A., Vasseur, P., Bennacer, R., Beji, H.: Natural convection of a two-component fluid in porous media bounded by tall concentric vertical cylinders. J. Appl. Mech. **73**, 26–33 (2006)

Boutana, N., Bahloul, A., Vasseur, P., Joly, F.: Soret and double diffusive convection in a porous cavity. J. Porous Med. **1**, 41–57 (2004)

Chang, C.J., Lin, T.F., Yan, W.M.: Natural convection in a vertical open tube resulting from combined buoyancy effects of thermal and mass diffusion. Int. J. Heat Mass Transf. **29**, 1543–1552 (1986)

Chen, F., Chen, C.F.: Double diffusive fingering convection in a porous medium. Int. J. Heat Mass Transf. **36**, 739–807 (1993)

Chen, S., Toolke, J., Krafczyk, M.: Numerical investigation of double-diffusive (natural) convection in vertical annuluses with opposing temperature and concentration gradients. Int. J. Heat Fluid Flow **31**, 217–226 (2010)

De Groot, S.R., Mazur, P.: Non equilibrium thermodynamics. North-Holland Pub, Amsterdam (1969)

Goyeau, B., Songbe, J.P., Gobin, D.: Numerical study of double diffusive convection in a porous cavity using Darcy-Brinkman. Int. J. Heat Mass Transf. **39**, 1363–1378 (1996)

Joly, F., Vasseur, P., Labrosse, G.: Soret driven thermosolutal convection in a vertical enclosure. Int. Comm. Heat Mass Transf. **27**, 755–764 (2000)

Khanafer, K., Vafai, K.: Double diffusive mixed convection in a lid-driven enclosure filled with a fluid saturated porous medium. Numer. Heat Transf. **42**, 465–486 (2002)

Malashetty, M.S.: Anisotropic thermoconvective effects on the onset of double diffusive convection in a porous medium. Int. J. Heat Mass Transf. **39**, 2397–2401 (1993)

Mamou, M., Vasseur, P.: Thermosolutal bifurcation phenomena in porous enclosures subject to vertical temperature and concentration gradients. J. Fluid Mech. **395**, 61–87 (1999)

Mamou, M., Vasseur, P., Bilgen, E., Gobin, D.: Double-diffusive convection in an inclined slot filled with porous medium. Eur. J. Mech. B **14**, 629–652 (1995a)

Mamou, M., Vasseur, P., Bilgen, E.: Multiple solutions for double diffusive convection in a vertical porous enclosure. Int. J. Heat Mass Transf. **38**, 1787–1798 (1995b)

Mamou, M., Hasnaoui, A., Ahmamid, A., Vasseur, P.: Stability of double diffusive convection in an inclined slut filled with porous medium. Int. Com. Heat Mass Transf. **25**, 491–500 (1998a)

Mamou, M., Vasseur, P., Bilgen, E.: A Galerkin finite element study of the onset of double diffusive convection in an inclined porous enclosure. Int. J. Heat Mass Transf. **41**, 1513–1529 (1998b)

Mamou, M., Vasseur, P., Bilgen, E.: Double-Diffusive instability in a vertical porous enclosure. J. Fluid Mech. **368**, 263–289 (1998c)
Marcoux, M., Charrier-Mojtabi, M.C.: Diffusion thermogravitationnelle dans un mélange binaire saturant un espace annulaire poreux vertical. Entropie **218**, 8–12 (1999)
Marcoux, M., Karimi-Fard, M., Charrier-Mojtabi, M.: Naissance de la convection thermosolutale dans une cellule rectangulaire poreuse soumise a des flux de chaleur. Int. J. Therm. Sci. **38**, 258–266 (1999)
Masuda, Y., Yoneya, M., Ikeshoji, T., Kimura, S., Alavyoon, F., Tsukada, T., Hozawa, M.: Oscillatory double diffusive convection in a porous enclosure due to opposing heat and mass fluxes on the vertical walls. Int. J. Heat Mass Transf. **45**, 1365–1369 (2002)
Nield, D.A.: The thermohaline Rayleigh-Jeffreys problem. J. Fluid Mech. **29**, 545–558 (1967)
Patankar, S.: Numerical heat transfer and fluid flow. Hemisphere, Washington, DC (1980)
Poulikakos, D.: Double diffusive convection in a horizontal sparcely packed porous layer. Int. Commun. Heat Mass Transf. **13**, 587–598 (1986)
Rudraiah, H., Shirimani, P.K., Friedrich, R.: Finite amplitude convection in a two component fluid saturated porous layer. Int. J. Heat Mass Transf. **25**, 715–722 (1982)
Shipp, P.W., Shoukri, M., Carver, M.B.: Double diffusive natural convection in a closed annulus. Num. Heat Transf. **24**, 339–356 (1993)
Taslim, M.E., Narusawa, U.: Binary fluid convection and double-diffusive convection in porous medium. J. Heat Transf. **108**, 221–224 (1986)
Trevisan, O., Bejan, A.: Natural convection with combined heat and mass transfer. Int. J. Heat Mass Transf. **28**, 1597–1611 (1985)
Trevisan, O., Bejan, A.: Mass and heat transfer by natural convection in a vertical slot filled with porous medium. Int. J. Heat Mass Transf. **29**, 403–415 (1986)
Trevisan, O., Bejan, A.: Mass and heat transfer by high Rayleigh number convection in a porous medium heated from below. Int. J. Heat Transf. **30**, 2341–2356 (1987)
Yan, W.M., Lin, D.: Natural convection heat and mass transfer in vertical annuli with film evaporation. Int. J. Heat Mass Transf. **44**, 1143–1151 (2001)